Macromolecules

Article

pubs.acs.org/Macromolecules

Optical Activity of Heteroaromatic Conjugated Polymer Films Prepared by Asymmetric Electrochemical Polymerization in Cholesteric Liquid Crystals: Structural Function for Chiral Induction

Kohsuke Kawabata,[†] Masaki Takeguchi,[‡] and Hiromasa Goto[†,*]

[†]Division of Materials Science, Faculty of Pure and Applied Sciences, University of Tsukuba, Tsukuba, Ibaraki, 305-8573, Japan

[‡]Microstructure Characterization Platform Promotion Office, National Institute for Materials Science, Tsukuba, Ibaraki, 305-0047, Japan

Supporting Information

ABSTRACT: We electrochemically polymerized various achiral heteroaromatic monomers in left-handed helical cholesteric liquid crystal (CLC) media. Circular dichroism (CD) spectroscopy revealed that most of the resulting conjugated polymer films exhibited both the first negative and second positive Cotton effects near their absorption maxima. This indicates left-handed helical aggregation of the conjugated main chains, which is consistent with left-handed helical order of the CLC. This result suggests that the left-handed helical CLC environment induced left-handed helical aggregation of the polymers during the electrodeposition. However, CD intensity of the polymers depends on the structure of the parent monomers. Systematic investigation of the relationship between monomer structures and optical activity of the polymers indicates that linearity of the conjugated main chains and excluded volume interaction between the monomers and the CLC are important factors for producing optical activity of the polymers.

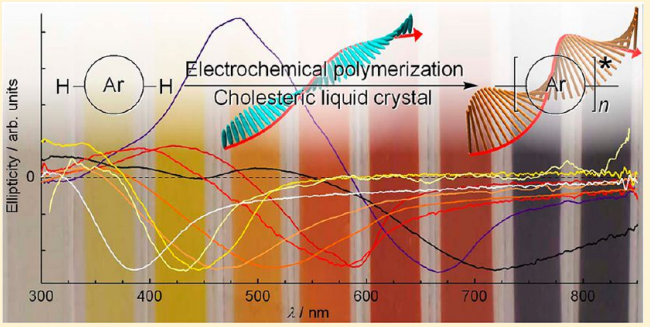

INTRODUCTION

Chiral polymers have attracted much interest because chiral molecular structures provide optical activity, such as circular dichroism (CD) and optical rotatory dispersion, nonlinear optical response, and chiral recognition and catalytic properties.[1−6]

Conjugated polymers are also of great interest because of their optical absorption and emission properties over the ultraviolet−visible and near-infrared regions, which can be modulated by designing the chemical structure.[7,8] For example, in the neutral state, poly-*p*-phenylenes, polyfluorenes and polycarbazoles absorb ultraviolet light and emit blue light,[9−11] and polythiophenes absorb and emit visible light,[12] while poly(3,4-ethylenedioxythiophene) (PEDOT), polyisothianaphthene, and donor−acceptor-type conjugated polymers exhibit absorption and emission bands that extend into the near-infrared region.[7,13,14] The absorption and emission properties of the conjugated polymers can also be modulated by chemical and electrochemical redox processes. Through the redox process conjugated polymers deform their conjugated backbones between the benzenoid structure in the neutral state into the quinonoid structure in the ionized state, accompanied by change in their electronic states.

For the construction of helically aggregated polymer structures, various chiral structural units have been introduced both to side chains and main chains.[15−20] However, recently, it has been reported that electrochemical polymerization of achiral monomers in a cholesteric liquid crystal (CLC) medium, which has helical molecular order, produced optically active conjugated polymer films.[21], The polymers thus prepared exhibited circular dichroism (CD) at the wavelengths where absorption due to the $\pi-\pi^*$ transition was observed, despite the absence of any chiral structure in the monomer repeating unit. This indicates that during the electrodeposition the chiral environment due to the CLC affects formation of 2-D intramolecular or 3-D intermolecular chiral structures that induce the optical activity of the resulting polymer. This method is referred to as "CLC asymmetric electrochemical polymerization". This is a unique method to prepare optically active conjugated polymers even from achiral monomers. Furthermore, thus-prepared conjugated polymer films show optical textures characteristic of the CLC medium used, indicating that conjugated polymer chains are mesoscopically oriented similarly to the periodically helical molecular order in the CLC. However, understanding details of the polymerization mechanism and supermolecular structure in the film is still insufficient and requires systematic studies.

Received: February 11, 2013
Revised: February 25, 2013

   dx.doi.org/10.1021/ma400302j | *Macromolecules* XXXX, XXX, XXX−XXX

Chart 1. Monomers Used for Asymmetric Electrochemical Polymerization

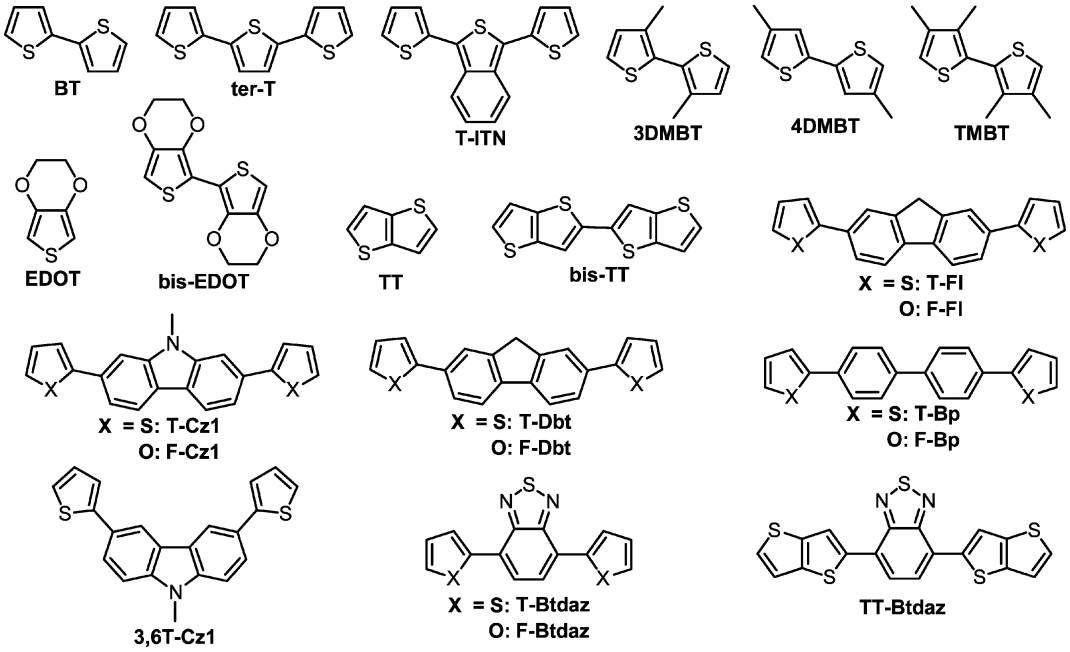

In this study, systematically designed monomers were used for the CLC asymmetric electrochemical polymerization to induce chiroptical activity in various conjugated polymers, in order to understand the aggregated polymer structure and the chiral induction mechanism in the CLC asymmetric electrochemical polymerization.

MONOMERS

2,2′-Bithiophene (**BT**), 2,2′:5′,2″-terthiophene (**ter-T**), 3,3′-dimethyl-2,2′-bithiophene (**3DMBT**), 4,4′-dimethil-2,2′-bithiophene (**4DMBT**), 3,4,3′,4′-tetramethyl-2,2′-bithiphene (**TMBT**), 1,3-di(2-thienyl)isothianaphthene (**T-ITN**), 3,4-ethylenedioxythiophene (**EDOT**), 2,2′-bis(3,4-ethylnenedioxythiophene) (**bis-EDOT**), thieno[3,2-*b*]thiophene (**TT**), 2,2′-bithieno[3,2-*b*]thiophene (**bis-TT**), 2,7-di(2-thienyl)fluorene (**T-Fl**), *N*-methyl-2,7-di(2-thienyl)carbazole (**T-Cz1**), 3,7-di(2-thienyl)dibenzothiophene (**T-Dbt**), 4,4′-di(2-thienyl)-biphenyl (**T-Bp**), 2,7-di(2-furyl)fluorene (**F-Fl**), *N*-methyl-2,7-di(2-furyl)carbazole (**F-Cz1**), 3,7-di(2-furyl)-dibenzothiophene (**F-Dbt**), 4,4′-di(2-furyl)biphenyl (**F-Bp**), 4,7-di(2-thienyl)-benzo[1,2,5]thiadiazole (**T-Btdaz**), 4,7-di(2-furyl)-benzo[1,2,5]thiadiazole (**F-Btdaz**), 4,7-bis-thieno[3,2-*b*]-thiophen-2-yl-benzo[1,2,5]thiadiazole (**TT-Btdaz**), and *N*-methyl-3,6-di(2-thienyl)carbazole (**3,6T-Cz1**) were each used as monomers for CLC asymmetric electrochemical polymerizations, which are listed in Chart 1. Synthetic routes to the monomers are described in Scheme 1.

Under the assumption that the electrochemical polymerization reaction proceeds via the radical coupling reaction as described by Genies et al.,[22] the reactive sites can be determined by spin-density distribution in the monomers in the radical cationic state.[23] Density functional theory (DFT) calculation revealed that in the potential reactive sites with eliminable protons in the monomers, external α-carbons of the heteroaromatic rings in the monomers have the highest spin density (Figure S1, Supporting Information). Specifically, the most reactive sites in the monomers in the radical cationic state are the external α-positions of the heteroaromatic rings. Thus, electrochemical polymerization of the monomers theoretically provides α-position-linked conjugate polymers.

CLC ELECTROLYTE SOLUTIONS

Generally, CLC phase can be induced from nematic liquid crystals (NLCs) by addition of a chiral compound, so-called chiral inducer. However, chiral inducers require good miscibility with the mother NLC. Otherwise, the addition of chiral compounds into the LC matrix may break the entire LC order like adding an impurity. In this study, cholesteryl oleyl carbonate (COC), a kind of cholesterol derivative, was used as a chiral inducer as reported in previous studies.[24] The CLC medium was prepared by addition of COC (136.2 mg, 0.20 mmol) as a chiral inducers to 4-cyano-4′-*n*-hexyl biphenyl (6CB) (1.32 g, 5.0 mmol). To the CLC medium (150 mg) was added tetrabutylammonium perchlorate (TBAP) (0.34 mg, 1.0 μmol) and monomers (1−8 μmol) to afford CLC electrolyte solutions (Table 1).

Liquid crystallinity of the CLC electrolyte solutions was confirmed by polarizing optical microscopy (POM) and differential scanning calorimetry (DSC). The electrolyte solutions were confirmed to maintain CLC phase even after the addition of TBAP and the monomers by POM observation of fingerprint textures that are characteristic of the CLC phase (Figure 1). In the POM observation for the CLC electrolyte solutions no precipitated TBAP or monomers were observed, indicating good homogeneity of the solution. DSC measurements show the phase transition temperatures of the CLC medium decreased slightly after addition of TBAP and **BT** (Figure S2, Supporting Information). In the temperature range from 16 to 27 °C, the CLC electrolyte solution exhibit a stable CLC phase under both cooling and heating. The helical half-pitch of the CLC medium at 22 °C was measured to be 1.14 μm by the Grandjean−Cano method.[25] This helical half-pitch length is long enough not to demonstrate any optical effects, such as selective reflection or optical band gap, at the absorption region of the resulting polymers (300−900 nm).

dx.doi.org/10.1021/ma400302j | *Macromolecules* XXXX, XXX, XXX−XXX

Scheme 1. Synthesis of Monomers

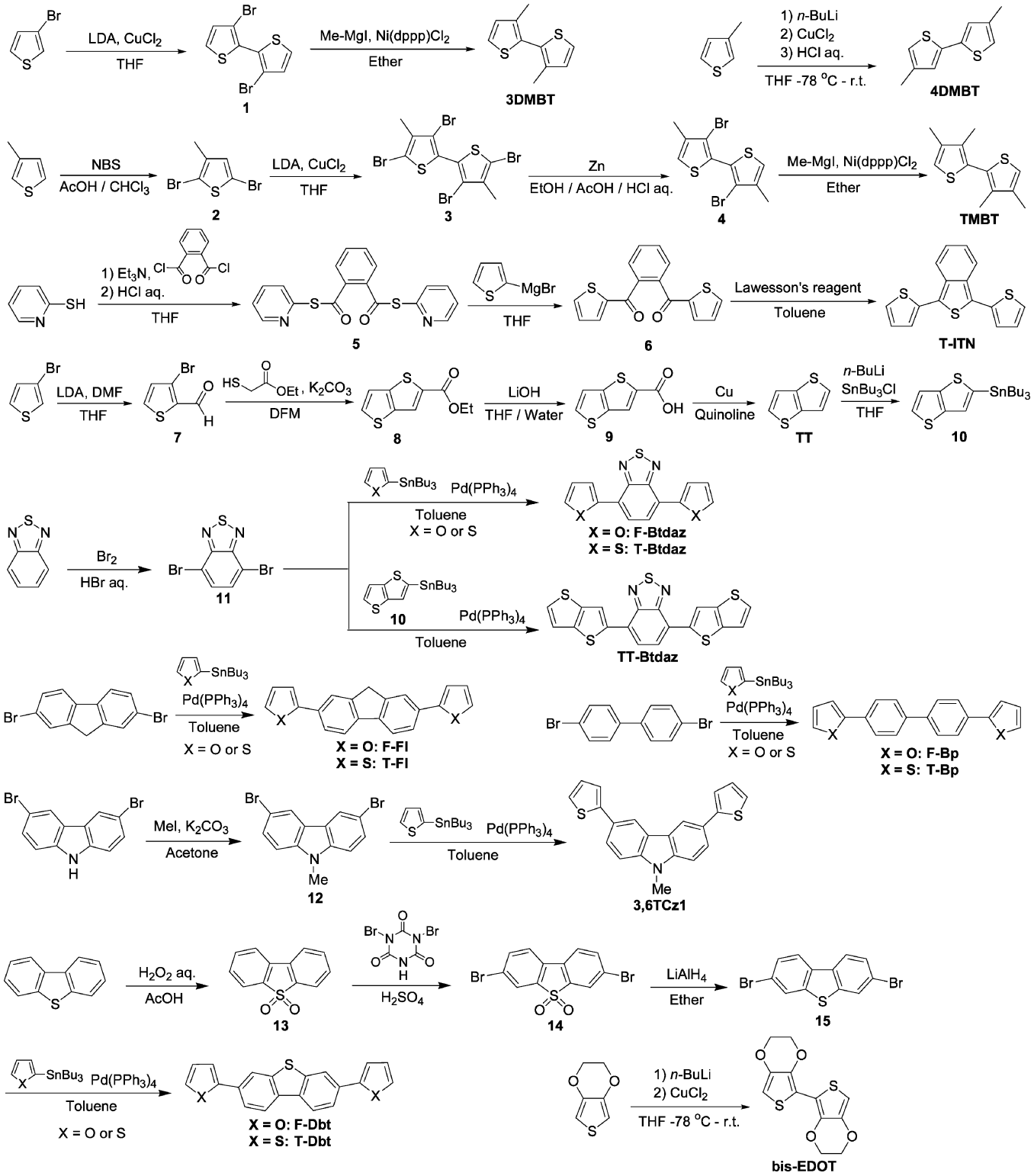

The helical twisting power of COC is estimated to be 11.4 μm^{-1}.

CLC ASYMMETRIC ELECTROCHEMICAL POLYMERIZATION

The CLC electrolyte solutions were injected between two indium−tin−oxide- (ITO-) coated glass electrodes, separated by a Teflon spacer of 0.20 mm thickness. The polymerization cell was first heated to form an isotropic phase of the CLC electrolyte solution, and then cooled and kept at 22 °C to maintain the CLC phase. In the polymerization cell helical axes of the CLC electrolyte were parallel to the substrate electrodes to form fingerprint textures. 4.0 V of direct current voltage was applied between the ITO electrodes to start electrochemical polymerization. After the reaction for 10−30 min, the CLC electrolyte solution was rinsed off with hexane and acetone to

dx.doi.org/10.1021/ma400302j | Macromolecules XXXX, XXX, XXX−XXX

Table 1. Constituents of Cholesteric Liquid Crystal Electrolytes

Constituents	Chemical Structure	Mole	Mass
Nematic liquid crystal	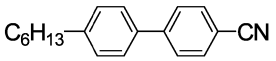	500 μmol	132 mg
Chiral inducer	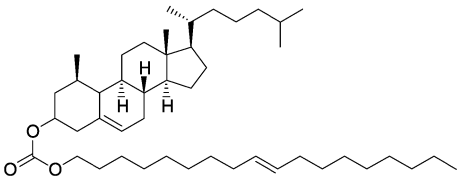	20 μmol	13.6 mg
Supporting salt	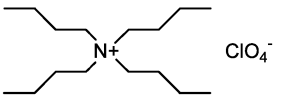	1 μmol	0.34 mg
Monomers	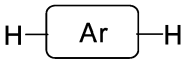	1 ~ 6 μmol	0.1 ~ 0.8 mg

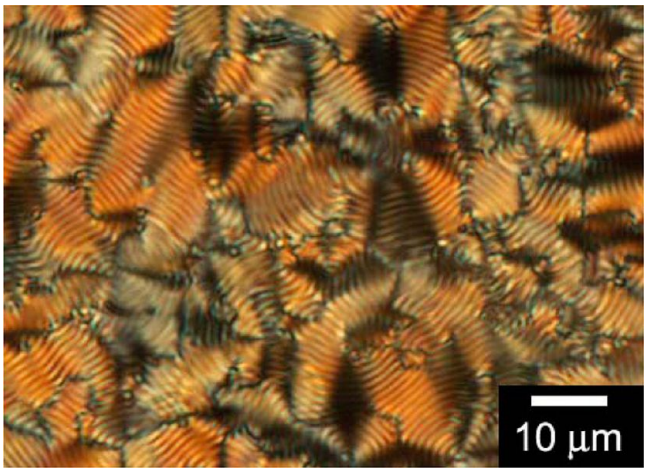

Figure 1. POM image of CLC electrolyte solution containing bithiophene (**BT**) monomer at 22 °C under crossed Nicols.

afford polymeric thin films on an anodic surface. The polymer films were fully reduced by exposure with hydrazine vapor prior to subsequent measurements.

The polymers prepared by the CLC asymmetric electrochemical polymerization were obtained as insoluble and infusible films on ITO glass electrodes. According to the DFT calculation results, polymerization reactions proceed via a radical coupling reaction between the α-positions of the heteroaromatic rings. In IR spectra of the polymers, absorption bands due to α-position C−H out-of-plane bending vibration (δ_{C-H}) of the heteroaromatic monomers disappeared after electrochemical polymerization (Figures S3 and S4, Supporting Information). This elucidates that the polymers grew via coupling between the α-position of the monomers. IR spectra of **poly(ter-T)** show a similar shape to the spectrum of **poly(ter-T)** prepared in acetonitrile, indicating that the polymerization reaction in this study proceeds in a similar way to the conventional method using common organic solvents (Figure S5, Supporting Information). Furthermore, the absence of absorption bands at 2230 and 1740 cm^{-1} due to C≡N stretching ($\nu_{C\equiv N}$) of 6CB and C═O stretching ($\nu_{C=O}$) of COC, respectively, indicates that the CLC solvent was completely removed after polymerization.

Molecular weight of the polymers was evaluated by matrix-assisted laser desorption ionization time-of-flight mass spectroscopy (MALDI-TOF-MS) using dithranol as a matrix. The spectra of the polymers show periodic patterns that correspond to molecular weights of the monomer repeating units (Figures S6 and S7, Supporting Information). The spectra show low average molecular weights; however, these spectra can only detect low molecular weight fractions.

■ OPTICAL PROPERTIES OF THE POLYMERS

CD and UV−vis spectra of polymer films prepared by the CLC asymmetric electrochemical polymerization are shown in Figure 2. Linear dichroism of the polymers were evaluated to be negligible intensity against CD observed as shown in Figure S10, Supporting Information, and removed from the CD spectra. **Poly(BT)** and **poly(ter-T)** synthesized in this study exhibited optical properties consistent with those of the same polymers previously synthesized by using similar methods to this study.[24,26] **Poly(BT)** and **poly(ter-T)** in this study show different absorption maxima around 470 and 490 nm, respectively, despite the same chemical structure of the resulting polymers (Figure 2a). This different effective conjugation length is caused by different reactivity of the monomer in the radical cationic state. It has been previously reported that in electrochemical polymerization, **ter-T** is less reactive than **BT** due to delocalization of π-electrons over the entire molecule. The low reactivity of **ter-T** results in lower

dx.doi.org/10.1021/ma400302j | Macromolecules XXXX, XXX, XXX−XXX

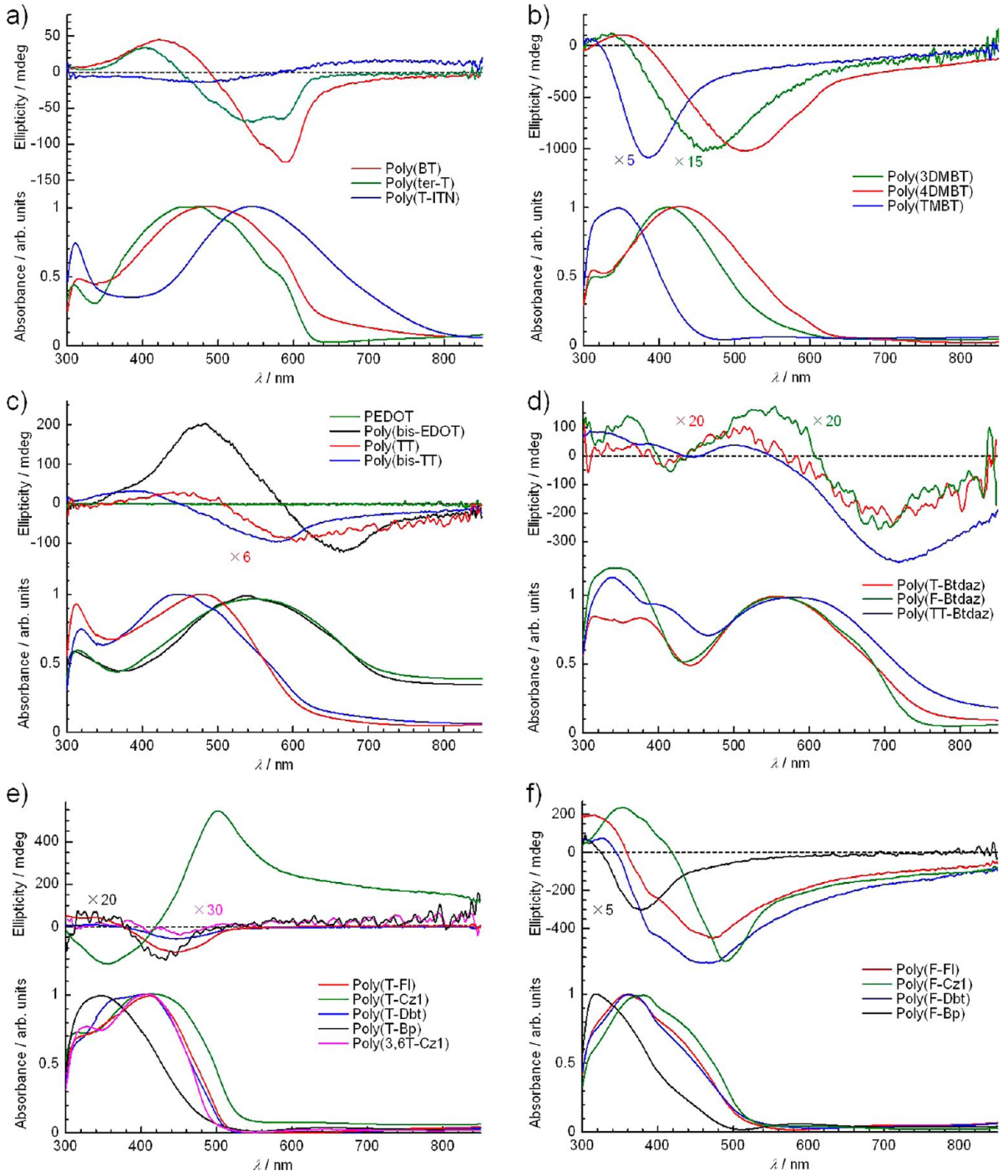

Figure 2. CD (top) and UV−vis (bottom) spectra of the polymer in the neutral state.

molecular weight of polythiophene than that prepared from **BT**.[27] The difference in the molecular weights of the polymers is also indicated by the difference in their IR spectra. The IR spectra of **poly(ter-T)** showed more intense absorption (at 693 cm^{-1}) due to out-of-plane C−H vibration (δ_{C-H}) at the α-position of thiophene rings than did **poly(BT)**, which indicates that **poly(ter-T)** has more unreacted terminal α-positions than **poly(BT)** (Figure S3a,b, Supporting Information). As a result, **poly(ter-T)** shows several absorption shoulders due to the well-defined low molecular weight polymers, while **poly(BT)** shows the absorption maximum and onset at longer wavelengths than **poly(ter-T)**. In CD spectra, **poly(ter-T)** and **poly(BT)** show bisignate Cotton effect near their absorption maximum wavelengths. These spectra are similar to those of previously reported helically aggregated polythiophenes.[28,29] This type of bisignate Cotton effect represents the chiral exciton coupling via Davydov splitting,[30] indicating chiral aggregation of polythiophene backbones. **Poly(ter-T)** and **poly(BT)** show first negative and second positive Cotton effects, indicating that polythiophene backbones form left-handed helical aggregation.[30] This left-handed helical aggregation is consistent with the left-handed helical order of the CLC medium consisting of 6CB and COC. On the contrary, **poly(T-ITN)** shows first positive and second negative Cotton effect at

dx.doi.org/10.1021/ma400302j | *Macromolecules* XXXX, XXX, XXX−XXX

around 550 nm of absorption maximum wavelength, indicating right-handed helical aggregation of the conjugated backbone.

Poly(3DMBT) and **poly(4DMBT)** show different absorption maxima at around 430 and 410 nm, respectively, despite the same chemical structure of head-to-head and tail-to-tail poly(methylthiophene) backbone (Figure 2b). The difference can be explained by two possible structural defects in the **poly(3DMBT)** backbones. One is $\alpha-\beta$ linkage defects due to potential reactivity at uncapped external β-positions of **3DMBT**,[31] while, in electrochemical polymerization of **4DMBT**, methyl substituents at external β-positions prevent formation of $\alpha-\beta$ linkage defects. The other possible structural defect in **poly(3DMBT)** is syn-defects which can be caused both in the monomer units and between the monomer units. The syn-defects in the monomer units are spontaneously formed because syn-conformation is energetically favorable to anticonformation for **3DMBT** in the neutral state, while anticonformation is favorable for **4DMBT** in the neutral state, according to inter-ring rotation energy profiles calculated by the DFT method (Figure 3). In the radical cationic states,

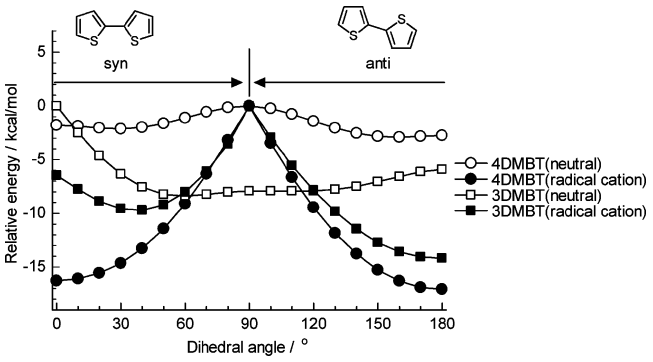

Figure 3. Energy profiles for inter-ring rotation of **4DMBT** in the neutral (open circle) and radical cationic (solid circle) state and **3DMBT** in the neutral (open square) and radical cationic (solid square) state calculated by DFT method (B3LYP-6-31G*). Syn-conformation: from 0° to 90°. Anticonformation: from 90° to 180°.

anticonformation is energetically favorable to syn-conformation for both **3DMBT** and **4DMBT**; however, there is a high energy barrier between syn- and anticonformation, more than 10 kcal mol^{-1}. Therefore, according to the Franck–Condon principle, once syn-**3DMBT** in the neutral state is electrochemically oxidized, **3DMBT** rarely reforms its syn-conformation into anticonformation. Another kind of syn-defect can be formed between the monomer units during the radical coupling reaction, which is more easily formed in **3DMBT** than **4DMBT** because of the steric hindered methyl substituents at the external β-positions of **4DMBT**. Thus, **poly(3DMBT)** has more structural defects in the conjugated backbone than **poly(4DMBT)**, resulting in shortening its effective conjugation length. **Poly(TMBT)** shows an absorption maximum at 346 nm, which is shorter than that of **poly(3DMBT)** and **poly(4DMBT)**. This is because **poly(TMBT)** has two steric hindered methyl groups per one thiophene unit to increase dihedral angles between thiophenes.

In the CD spectra, **poly(3DMBT)**, **poly(4DMBT)**, and **poly(TMBT)** exhibit bisignate Cotton effects with different intensities, which have first negative and second positive Cotton effects. The relatively small CD intensity of **poly(3DMBT)** is consistent with structural defects in the conjugated main chain. These three spectra are not zero-crossing at absorption maxima, while unsubstituted **poly(BT)** and **poly(ter-T)** show zero-crossing points at absorption maxima in the CD spectra. This indicates that in the CD spectra of **poly(3DMBT)**, **poly(4DMBT)**, and **poly(TMBT)**, a monosignate negative Cotton effect due to one-handed twisted conjugated single chains is superimposed on the bisignate Cotton effect due to helical aggregation between the conjugated chains. The one-handed twisted conformation in the methyl-substituted polythiophenes is caused by steric hindered methyl groups, while unsubstituted polythiophene have coplanar conjugated structures, which is supported by the DFT calculation (Figure S8, Supporting Information).

Poly(TT) and **poly(bis-TT)** show almost identical absorption spectra, and yield first negative and second positive Cotton effect at around their absorption maximum wavelengths. However, the CD intensity of **poly(TT)** is smaller than that of **poly(bis-TT)** (Figure 2c). To the contrary, **poly(bis-EDOT)** and **PEDOT** show significant difference in CD spectra despite the same chemical structure and UV–vis and IR absorption spectra (Figure 2c and Gigure S3g,h, Supporting Information). In the CD spectra, **poly(bis-EDOT)** shows distinct first negative and second positive Cotton effect at around its absorption maximum (550 nm), while **PEDOT** shows no detectable Cotton effect. This significant difference in optical activity, in spite of the same UV–vis and IR absorption, suggests that the choice of parent monomers is quite important for the construction of chiral polymer structure during CLC asymmetric electrochemical polymerization.

Figure 2d shows CD and UV–vis absorption spectra of three donor–acceptor (D-A)-type conjugated polymers, **poly(T-Btdaz)**, **poly(F-Btdaz)**, and **poly(TT-Btdaz)**. **Poly(T-Btdaz)** and **poly(F-Btdaz)** show intermolecular charge transfer absorption bands at around 560 nm, which are characteristic of D–A conjugated polymers. At short wavelengths (300 nm ~400 nm), **poly(T-Btdaz)** and **poly(F-Btdaz)** show one and two absorption bands, respectively. **Poly(TT-Btdaz)** shows a charge-transfer-type band at a little longer wavelength than **poly(T-Btdaz)** and **poly(F-Btdaz)** (580 nm), indicating that the bis(thienothiophene) unit functions as a stronger donor than bithiophene or bifuran. In the CD spectra, three D–A polymers show two or three bisignate Cotton effects near absorption maxima. The bisignate Cotton effects at long wavelengths are more intense than those at short wavelengths, although the absorption intensities at both long and short wavelengths are at the same level. Among the D–A polymers, **poly(TT-Btdaz)** shows much stronger CD than **poly(T-Btdaz)** and **poly(F-Btdaz)**.

Parts e and f of Figure 2 show CD and UV–vis spectra of the polymers prepared from thiophene- and furan-disubstituted four-ring monomers, respectively. These polymers show similar absorption bands near 300 nm -500 nm because of the similar chemical structure. However the biphenyl-based polymers, **poly(T-Bp)** and **poly(F-Bp)**, show maximum absorption bands at shorter wavelengths than the others. This is because the unbridged biphenyl is less planar and has less effective conjugation than bridged biphenyl systems such as fluorene, carbazole, and dibenzothiophene. Additionally, **poly(T-Cz1)** and **poly(F-Cz1)** have slightly longer absorption maximum wavelengths than the other biphenyl systems.

In the CD spectra, these polymers, except for **poly(T-Cz1)** and **poly(3,6T-Cz1)**, show first negative and second positive Cotton effects around their absorption bands. On the contrary,

dx.doi.org/10.1021/ma400302j | *Macromolecules* XXXX, XXX, XXX–XXX

poly(T-Cz1) shows intense first positive and second negative Cotton effect, while **poly(3,6T-Cz1)** shows no clear Cotton effect.

DISCUSSION

Most of the polymers in this study showed the first negative and the second positive Cotton effects (negative couplet) in their CD spectra around their maximum absorption wavelengths. These Cotton effects are characteristic of Davydov splitting-type CD by chiral exciton coupling between left-handed helically ordered chromophores. In the conjugated polymers, conjugated backbones function as chromophores, whose transition moments are along the conjugated backbones. Therefore, the negative couplets in the CD indicate that the conjugated polymers form left-handed helical order of their rigid conjugated main chains in their aggregated state, as do the CLC molecules (Figure 4).[30]

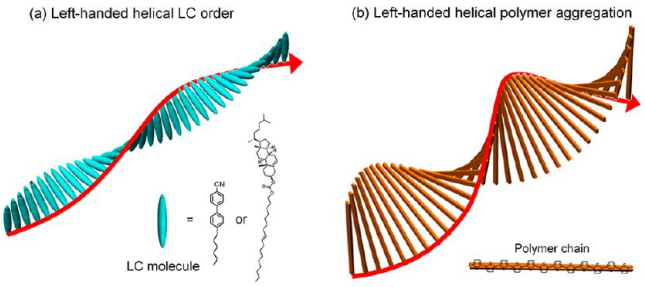

Figure 4. Illustration of the left-handed helical LC-order (a) and aggregated polymer structure (b) in this study.

This helical order of the polymers is supported by the periodic birefringence structure observed in POM images of the polymer films as shown in Figure 5. The POM images for

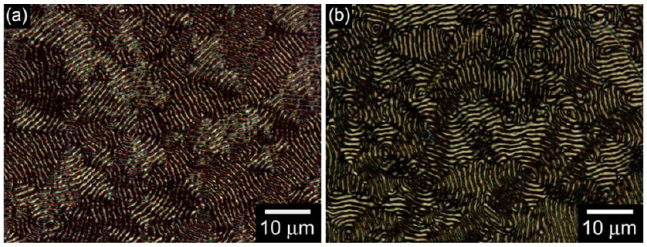

Figure 5. POM images under crossed Nicols of **poly(4DMBT)** (a) and **poly(bis-EDOT)** (b) films prepared by CLC asymmetric electrochemical polymerization.

polymer films under crossed Nicol show fingerprint texture, which is similar to that of the CLC solvent used. It is well-known that CLCs form periodic helical molecular order that shows fingerprint textures, in which the width of each stripe corresponds to the distance required for the LC director to rotate 180°. The distance is the "helical half-pitch". Therefore, the fingerprint texture of the polymer films similar to that of the CLC strongly suggests periodic helical orientation of the polymer chains. Besides, the helical half-pitch in the fingerprint texture of the polymer films is in good agreement with that of the CLC solvent.

For the construction of the helical aggregation during the polymerization reaction, the chiral environment induced the polymers to form chiral 3-D structures through anisotropic interaction between the chiral environment and the dissolved monomers and growing oligomers. One of the most important anisotropic interactions between the CLC and the solvated monomers and oligomers can be excluded volume interaction. Generally, a large length/diameter (L/D) ratio for a molecule dissolved in LC solvent causes strong excluded volume interaction, while a low L/D ratio results in little anisotropic interaction. The small CD in **poly(TT)**, **poly(T-Btdaz)**, **poly(F-Btdaz)**, and **poly(3,6T-Cz1)**, and no CD in **PEDOT**, can be explained by the small L/D ratios of the parent monomers resulting in little anisotropic interaction during polymerization.

Another important factor for enhancing CD due to the chiral exciton coupling in the helical aggregation can be the angle of the optical transition dipole moment relative to the polymer chain axis director. For example, zigzag- shaped conjugated polymers are unable to demonstrate one-handed chiral exciton coupling at each local point even if the polymer chains form the helical aggregation as a whole (Figure 6). This is because the

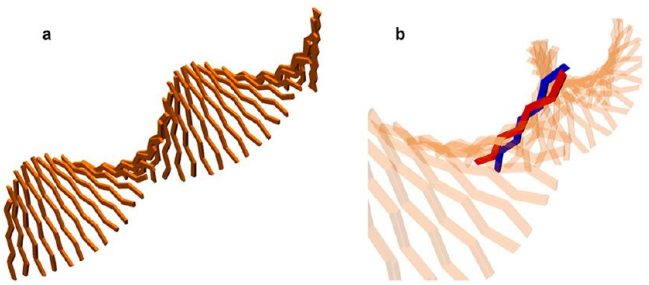

Figure 6. Illustration of the left-handed helically aggregated structure of the zigzag-shaped polymers (a and b). The red and blue chains are next to each other (b).

zigzag- conjugated polymer chains are unable to form one-handed helical conformation at each local point, resulting in fluctuation of the angle between their optical transition dipole moments, as shown in Figure 6b. Such fluctuation of the angle between the chromophore may decrease the total CD intensity. Thus, the small CD intensities of **poly(T-Btdaz)**, **poly(F-Btdaz)**, and **poly(3,6T-Cz1)** compared to **poly(TT-Btdaz)** and **poly(T-Cz1)** can be due to their zigzag-conjugated chains as well as the small L/D ratio of the monomers (Figure 7).

To the contrary, **poly(T-ITN)** and **poly(T-Cz1)** show the first positive and second negative Cotton effect (positive couplet) in the CD spectra, indicating right-handed helical aggregation. This result is inconsistent with the left-handed helical sense of the CLC solvent. However, elongation of the alkyl chain attached to the nitrogen atom of **poly(T-Cz1)** results in the opposite sign of CD of the polymers (**poly(T-Cz*m*)** m = 2−8) as shown in Figure 8a. A significant spectral difference is observable between **poly(T-Cz1)** and **poly(T-Cz2)** despite only one-carbon difference between the monomers. Interestingly, the CD intensity and absorption bandwidths of the **poly(T-Cz*m*)** decrease with the increase of the number of carbon atoms in the alkyl chains. A series of furan derivatives **poly(F-Cz*m*)** (m = 1−6) also show such spectral variation; however, they show only negative couplets (Figure 8b). This spectral variation can be explained by two mechanisms. One is that sterically hindered side alkyl chains suppress the interchain exciton coupling. The other is that lowering the L/D ratio of the monomers due to laterally attached alkyl chains decreases the anisotropic interaction

dx.doi.org/10.1021/ma400302j | *Macromolecules* XXXX, XXX, XXX−XXX

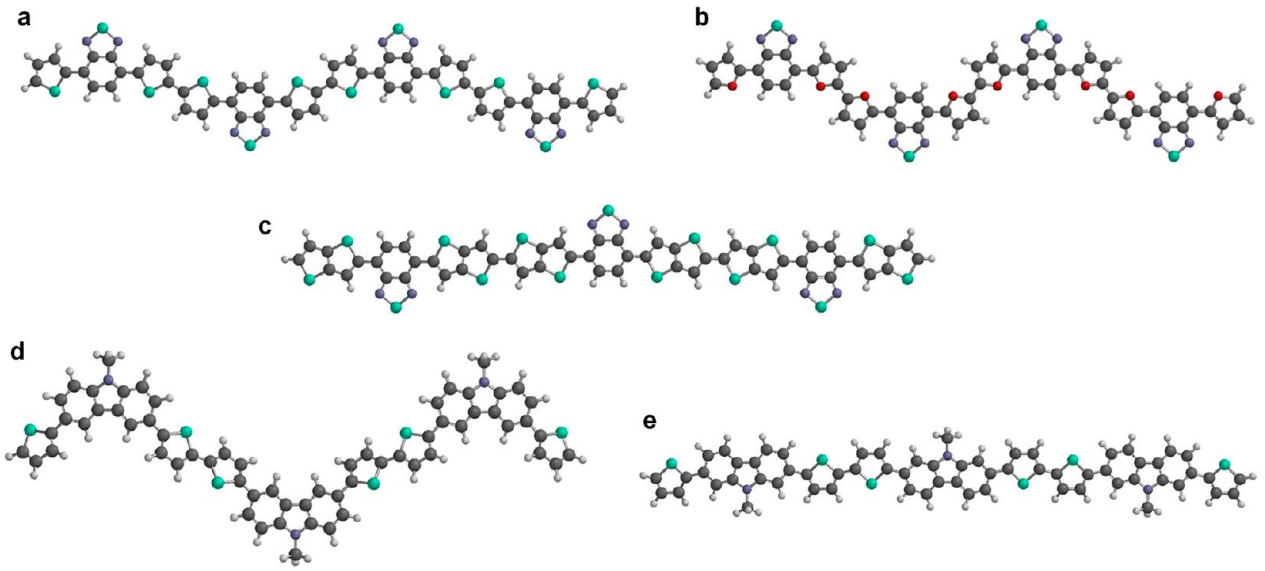

Figure 7. Optimized geometry of the model oligomers for **poly(T-Btdaz)** (a), **poly(F-Btdaz)** (b), **poly(TT-Btdaz)** (c), **poly(3,6T-Cz1)** (d), and **poly(T-Cz1)** (e) calculated by DFT method (B3LYP-6-31G*).

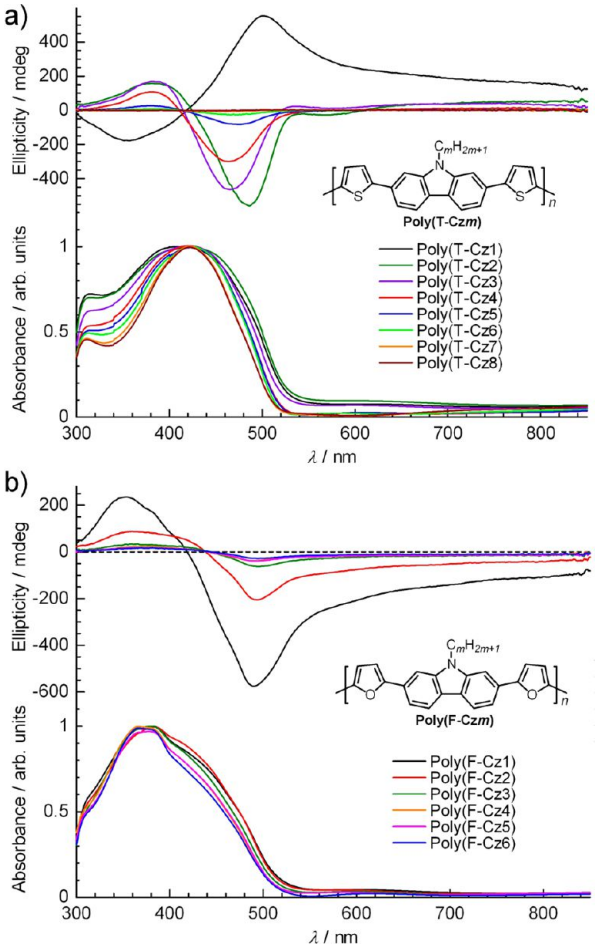

Figure 8. UV–vis (bottom) and CD (top) spectra of **poly(T-Czm)** (a) and **poly(F-Czm)** (b) in the reduced state.

between the monomers and the CLC during the polymerization reaction, resulting in disorder in the helical aggregation polymer structure.

To compare the aggregated structures of **poly(T-Czm)**, surface morphology of the polymers were observed by SEM (Figure 9). In the SEM images, **poly(T-Cz1)** forms nanoplates

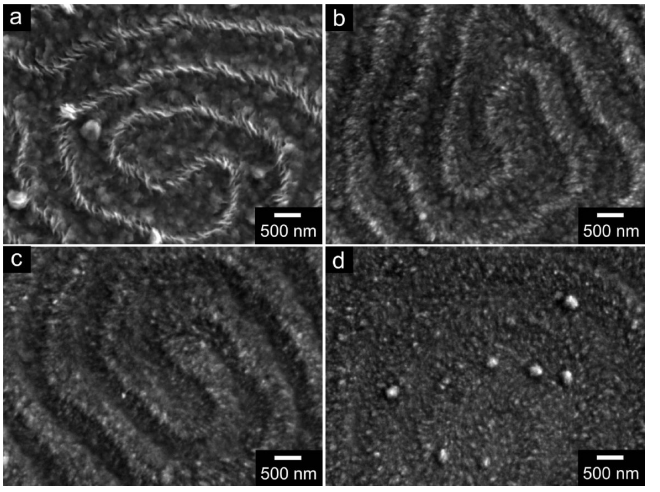

Figure 9. SEM images of **poly(T-Cz1)**, **poly(T-Cz2)**, **poly(T-Cz3)**, and **poly(T-Cz4)**.

which align along the fingerprint texture. This structure suggests two kinds of anisotropic growth of the **poly(T-Cz1)** in the CLC. First, the fingerprint textures of the polymers indicate the anisotropic growth of the polymers along the mesoscopically periodic helical order of the CLC during the polymerization. Second, the formation of nanoplates indicates strong anisotropic interaction between the polymers and oligomers through the deposition process. The nanoplates are one-handed helically stacked to form the fingerprint texture. Among the series of **poly(T-Czm)**, such nanoplate formation was observed only in **poly(T-Cz1)**. The positive couplet CD observed in **poly(T-Cz1)** can be derived from the right-handed helically distorted nanoplates; whereas **poly(T-Cz2)**, **poly(T-Cz3)**, and **poly(T-Cz4)** show globular surfaces forming convex-concave structures along the fingerprint texture. Additionally, the convex-concave fingerprint texture disappears with

dx.doi.org/10.1021/ma400302j | *Macromolecules* XXXX, XXX, XXX–XXX

the increase in the side alkyl chain length. **Poly(T-C*zm*)** with alkyl chains longer than pentyl group show globular surface and no fingerprint texture. The disappearance of the convex-concave structure in the polymers with long alkyl chains indicates that the lateral alkyl chain decreases anisotropic interaction between the chiral environment and the monomers and the growing oligomers due to the low L/D ratio of the monomers.

USE OF DIFFERENT CHIRAL INDUCERS

Cholesterol derivatives are often used as chiral inducers because their steroid skeletons function as a good mesogen with many asymmetric carbons. Likewise, synthetic chiral inducers require mesogens and some asymmetric carbons. As well as COC, cholesteryl pelargonate (CP) and 4′-(4-hexyloxy-benzoyloxy)-biphenyl-4-carboxylic acid-(*S*)-1-methyl-heptyl ester (**(*S*)-8BpB6**) in Chart 2 also function as chiral inducers in 6CB;

Chart 2. Chiral Inducers

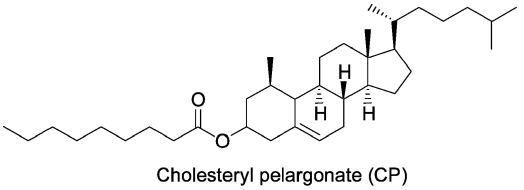

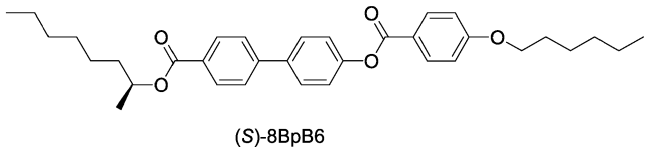

however, they have different helical twisting powers (β_M = 10.5 μm^{-1}, 19.5 μm^{-1}, respectively). **(*S*)-8BpB6** was synthesized via Mitsunobu reaction to introduce an symmetric carbon (Scheme 2). By using CP and **(*S*)-8BpB6** as chiral inducers two CLC electrolyte solutions were prepared as follows, to have the same helical half-pitch as the CLC containing COC in this study (ρ = 1.14 μm): to 6CB (132 mg, 500 μmol) was added CP (11.5 mg, 21.8 μmol) or **(*S*)-8BpB6** (6.1 mg, 11.5 μmol), TBAP (0.34 mg, 1.0 μmol), and **BT** (0.67 mg, 4.0 μmol) to afford CLC electrolyte solutions.

These two LC electrolyte solutions (CP/6CB and **(*S*)-8BpB6**/6CB) were confirmed to form a CLC phase at room temperature by POM observation. The helical senses of the two CLC electrolytes were determined by the contact method with COC/6CB as a left-handed helical standard CLC. The boundary area between the two new CLC electrolytes and COC/6CB were confirmed to exhibit continuous CLC phase by POM observation (Figure S9, Supporting Information). Therefore, CP/6CB and **(*S*)-8BpB6**/6CB CLC systems have left-handed helical molecular order.

In both these CLC solvents, as well as in the COC/6CB solvent, **BT** was electrochemically polymerized to form polymeric films. **Poly(BT)** films prepared in CP/6CB and **(*S*)-8BpB6**/6CB CLCs exhibit almost the same UV−vis absorption and CD spectra (Figure 10). COC and CP have

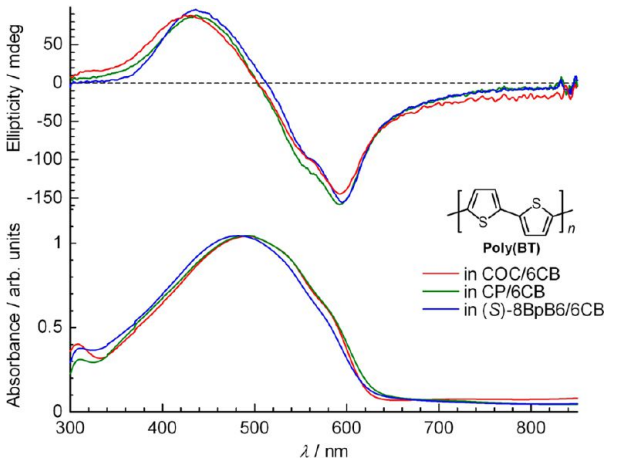

Figure 10. UV−vis (bottom) and CD (top) spectra of **poly(BT)** prepared in the CLCs with different chiral inducers, cholesteryl oleyl carbonate (red), cholesteryl pelargonate (green), and (*S*)-8BpB6 (blue) in the reduced state.

the same chiral steroid skeleton, while **(*S*)-8BpB6** has one asymmetric carbon next to an ester group. The similar CD spectra of the three **poly(BT)**s strongly suggest that the helically aggregated polymer structures were induced, not by chiral structural units of the chiral inducers, but by the helical molecular order of CLC phase.

CONCLUSIONS

A series of aromatic conjugated monomers were electropolymerized in a left-handed helical CLC medium consisting of 6CB and COC. Most of the resulting polymer films show Davydov splitting-type negative couplet near their absorption maximum wavelength in their CD spectra, which indicates left-handed helical aggregation of conjugated main chains. However, the CD intensities of the resulting polymers strongly depend on the parent monomer structures. The electrochemical polymerization of systematically designed monomers provided some guidelines for obtaining high optical activity of the polymers: (1) excluded volume interactions between

Scheme 2. Synthesis of the Chiral Inducer

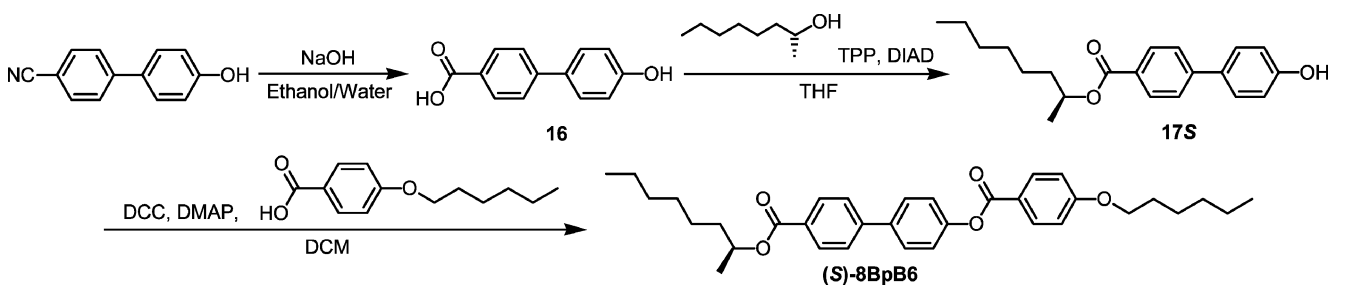

dx.doi.org/10.1021/ma400302j | *Macromolecules* XXXX, XXX, XXX−XXX

monomers and LC molecules are important; (2) a linear conjugated backbone of the resulting polymers is preferable; (3) a long alkyl chain can prevent chiral exciton coupling between the conjugated main chains. Furthermore, obtaining the same optical properties using different chiral inducers with the same helical half-pitch indicates that the driving force of the helical induction to the polymers is not the chiral structural units of the chiral inducers, but rather the helical molecular order of the CLC continuum.

MATERIALS

2,2′-Bithiophene, 2,2′:5′,2″-terthiophene, tetrabutylammonium perchlorate, cholesteryl oleyl carbonate, and cholesteryl pelargonate were purchased from Tokyo Chemical Industry (TCI). 3,4-Ethylenedioxythiophene was purchased from TCI and distilled prior to use. 4-Cyano-4′-*n*-hexyl biphenyl was purchased from Merck. 2,2′-Bithieno-[3,2-*b*]thiophene was purchased from Aldrich.

SYNTHESIS OF MONOMERS

T-C*z*m, **F-C*z*m**, **F-Bp**, and **F-Fl** monomers were previously synthesized by our group.[32−35]

3,3′-Dibromo-2,2′-bithiophene (1). To a solution of 3-bromothiophene (9.78 g, 60 mmol) in tetrahydrofuran (100 mL) was added lithium diisopropylamide (freshly prepared from diisopropylamine (8.4 mL, 60 mmol) and 1.6 M *n*-butyllithium in hexane (38 mL, 61 mmol) in tetrahydrofuran (20 mL)) dropwise over 15 min at −78 °C. After stirring for 1 h at −78 °C, $CuCl_2$ (8.07 g, 60 mmol) was added to the mixture in one portion, and the mixture was gradually warmed up to room temperature. After 6 h, the reaction was quenched with 1 M HCl(aq) (100 mL), and the mixture was extracted with dichloromethane, and the organic layer was dried over magnesium sulfate. The crude product was purified by column chromatography (eluent: hexane), and recrystallized from hexane/ethanol) to afford a pale yellow solid (6.36 g, 19.6 mmol, yield = 65%). ^{1}H NMR (400 MHz; $CDCl_3$; TMS): δ 7.08 (d, 2H, J = 5.4 Hz), 7.41 (d, 2H, J = 5.4 Hz). ^{13}C NMR (100 MHz; $CDCl_3$; TMS): δ 112.65, 127.53, 128.89. 130.81.

3,3′-Dimethyl-2,2′-bithiophene (3DMBT). To a solution of 3,3′-dibromo-2,2′-bithiophene (**1**) (1.30 g, 4.0 mmol) and dichloro-(1,3-bis(diphenylphosphino)propane)nickel (0.054 g, 0.10 mmol) in ether (20 mL) was added methylmagnesium iodide (freshly prepared from iodomethane (2.27 g, 16.0 mmol) and magnesium (0.41 g, 17.0 mmol) in ether (10 mL)) dropwise at 0 °C, and the reaction mixture was gradually warmed up to room temperature. After 6 h, the reaction was quenched with methanol (3 mL) carefully. The mixture was extracted with ether and water, and the organic layer was dried over magnesium sulfate. The crude product was purified by silica gel column chromatography (eluent: hexane) to afford colorless liquid (0.70 g, 3.6 mmol, yield = 90%). ^{1}H NMR (400 MHz; $CDCl_3$; TMS): δ 2.17 (s, 6H), 6.92 (d, 2 H, J = 4.8 Hz), 7.26 (d, 2H, J = 4.8 Hz). ^{13}C NMR (100 MHz; $CDCl_3$; TMS): δ 14.63, 124.94, 129.37, 129.98, 136.48.

4,4′-Dimethyl-2,2′-bithiophene (4DMBT). To a solution of 3-methylthiophene (3.93 g, 40 mmol) in dried THF (100 mL) was added *n*-butyllithium (1.6 M in hexane) (26.3 mL, 42 mmol) dropwise over 10 min at −78 °C. After stirring at −78 °C for 1 h, $CuCl_2$ (5.65 g, 42 mmol) was added in one portion, and the mixture was gradually warmed up to room temperature. After stirring overnight, aqueous HCl solution (2M, 80 mL) was added. The mixture was extracted with ether and the organic layer was dried over magnesium sulfate. The mixture was purified by silica gel column chromatography (eluent: hexane) to afford a white solid (2.87 g, 69% purity by ^{1}H NMR) which contained a head-to-tail compound. Further purification by recrystallization from methanol gave a colorless crystal (1.26 g, 6.5 mmol, yield = 33%). ^{1}H NMR (400 MHz; $CDCl_3$; TMS): δ 2.24 (d, 6H, −C*H*3, J = 1.0 Hz), 6.76 (s, 2H, 3,3′-*H*(thiophene)), 6.95 (d, 2H, 5,5′-*H*(thiophene), J = 1.0 Hz). ^{13}C NMR (100 MHz; $CDCl_3$; TMS): δ 15.73, 119.44, 125.77, 137.35, 138.33.

2,5-Dibromo-3-methylthiophene (2). To a solution of 3-methylthiophene (9.8 g, 100 mmol) in acetic acid (50 mL) and chloroform (50 mL) was added *N*-bromosuccinimide (37.4 g, 210 mmol) slowly at room temperature. The mixture was refluxed at 80 °C for 6 h. After the reaction, the mixture was extracted with chloroform and NaOH(aq) and washed with water, and the organic layer was dried over magnesium sulfate. The crude product was purified by column chromatography (eluent: hexane) to afford a colorless liquid (22.9 g, 90 mmol, yield = 90%). ^{1}H NMR (400 MHz; $CDCl_3$; TMS): δ 2.15 (s, 3H), 6.76 (s, 1H). ^{13}C NMR (100 MHz; $CDCl_3$; TMS): δ 15.13, 108.36, 110.12, 131.86, 138.05.

3,3′,5,5′-Tetrabromo-4,4′-dimethyl-2,2′-bithiophene (3). To a solution of lithium diisopropylamide (freshly prepared from diisopropylamine (14.3 mL, 102 mmol) and 1.6 M *n*-butyllithium in hexane (58.4 mL, 94 mmol) in tetrahydrofuran (180 mL)) was added 2,5-dibromo-3-methylthiophene (**2**) (21.8 g, 85 mmol) dropwise over 10 min at −78 °C. After stirring for 2 h at −78 °C, $CuCl_2$ (8.07 g, 60 mmol) was added to the mixture in one portion, and the mixture was gradually warmed up to room temperature. After 6 h, the reaction was quenched with 1 M HCl(aq) (100 mL), and the mixture was extracted with chloroform, and the organic layer was dried over magnesium sulfate. The crude product was purified by recrystallization from chloroform to afford a white solid (18.4 g, 36 mmol, yield = 85%). ^{1}H NMR (400 MHz; $CDCl_3$; TMS): δ 2.26 (s, 6H). ^{13}C NMR (100 MHz; $CDCl_3$; TMS): δ 16.29, 111.08, 114.92, 128.27, 137.27.

3,3′-Dibromo-4,4′-dimethyl-2,2′-bithiophene (4). A solution solution of 3,3′,5,5′-Tetrabromo-4,4′-dimethyl-2,2′-bithiophene (**3**) (16.3 g, 32 mmol) in ethanol (100 mL), 0.3 M HCl(aq) (20 mL), and acetic acid (20 mL) was refluxed at 110 °C, and zinc dust (5.9 g, 90 mmol) was added portionwise to the mixture. After 3 h, the zinc dust was removed by hot filtration, and the filtrate was cooled in a fridge. The precipitate was recovered by filtration and purified by recrystallization from ethanol to afford colorless crystal (10.1 g, 28 mmol, yield = 88%). ^{1}H NMR (400 MHz; $CDCl_3$; TMS): δ 2.28 (d, 6H, J = 1.1 Hz), 7.13 (quartet, 2H, J = 1.1 Hz). ^{13}C NMR (100 MHz; $CDCl_3$; TMS): δ 16.70, 115.85, 122.28, 129.39, 137.63.

3,3′,4,4′-Tetramethyl-2,2′-bithiophene (TMBT). To a solution of 3,3′-dibromo-4,4′-dimethyl-2,2′-bithiophene (**4**) (1.41 g, 4.0 mmol) and dichloro(1,3-bis(diphenylphosphino)propane)nickel (0.054 g, 0.10 mmol) in ether (18 mL) was added methylmagnesium iodide (freshly prepared from iodomethane (2.27 g, 16.0 mmol) and magnesium (0.41 g, 17.0 mmol) in ether (10 mL)) dropwise at 0 °C, and the reaction mixture was gradually warmed up to room temperature. After 6 h, the reaction was quenched with methanol (3 mL) carefully. The mixture was extracted with ether and water, and the organic layer was dried over magnesium sulfate. The crude product was purified by silica gel column chromatography (eluent: hexane) to afford a white solid (0.83 g, 3.7 mmol, yield = 93%). ^{1}H NMR (400 MHz; $CDCl_3$; TMS): δ 2.03 (s, 6H), 2.19 (d, 6H, J = 0.8 Hz), 6.94 (d, 2H, J = 0.8 Hz). ^{13}C NMR (100 MHz; $CDCl_3$; TMS): δ 13.37, 15.40, 120.57, 130.18, 136.14, 137.84.

Benzene-1,2-dicarbothioic acid di-*S*-pyridin-2-yl Ester (5). To a solution of pyridine-2-thiol (6.67 g, 60 mmol) and triethylamine (10 mL, 72 mmol) in tetrahydrofuran (100 mL) was added a solution of phthaloyl dichloride (6.09 g, 30 mmol) in tetrahydrofuran (90 mL) all at once with vigorous stirring at 0 °C, and then the reaction was immediately quenched with 1 wt % HCl(aq) (400 mL). The mixture was extracted with chloroform, and washed with 10 wt % NaOH(aq), and the organic layer was dried over magnesium sulfate. The crude product was purified by recrystallization from chloroform/ethyl acetate to afford pale yellow solid (6.79 g, 19 mmol, yield = 64%). ^{1}H NMR (400 MHz; $CDCl_3$; TMS): δ 7.31 (ddd, 2H, J = 2.0, 5.2, 7.0 Hz), 7.65 (dd, 2H, J = 3.2, 5.8 Hz), 7.74−7.80 (m, 4H), 7.89 (dd, 2H, J = 3.2, 5.8 Hz), 8.64 (ddd, 2H, J = 0.8, 2.0, 4.6 Hz). ^{13}C NMR (100 MHz; $CDCl_3$; TMS): δ 123.74, 128.62, 130.45, 132.03, 136.82, 137.31, 150.41, 151.35, 190.23.

1,2-Di(2-thienoyl)benzene (6). To a solution of benzene-1,2-dicarbothioic acid di-S-pyridin-2-yl ester (**5**) (3.52 g, 10 mmol) in dry THF was added 2-thienyl magnesium bromide (20 mmol) in THF solution dropwise at 0 °C over 10 min. After stirring at 0 °C for 30

dx.doi.org/10.1021/ma400302j | *Macromolecules* XXXX, XXX, XXX−XXX

min, the reaction was quenched with 10% HCl aqueous solution (100 mL). The mixture was extracted ether and washed with 10% NaOH aqueous solution and water. The organic layer was dried over magnesium sulfate. The solvent was removed under vacuum to afford a orange solid (2.92 g, 9.8 mmol, yield = 98%). ^{1}H NMR (400 MHz; $CDCl_3$; TMS): δ 7.07 (dd, 2H, 4,4′-*H*(thiophene), J = 3.6, 4.2 Hz), 7.47 (dd, 2H, 3,3′-*H*(thiophene), J = 1.1, 4.2, Hz), 7.64 (dd, 2H, 4,5-*H*(benzene), J = 3.2, 5.8 Hz), 7.66 (dd, 2H, 5,5′-*H*(thiophene), J = 1.1, 5.0 Hz), 7.74 (dd, 2H, 3,6-*H*(benzene), J = 3.2, 5.8 Hz). ^{13}C NMR (100 MHz; $CDCl_3$; TMS): δ 121.98, 129.18, 130.58, 134.92, 135.09, 139.31, 144.03, 188.25.

1,3-Di(2-thienyl)isothianaphthene (T-ITN). A solution of 1,2-di(2-thienoyl)benzene (**6**) (0.60 g, 2.0 mmol) and Lawesson's reagent (1.09 g, 2.7 mmol) in toluene (70 mL) was refluxed at 100 °C for 2 h. After the reaction, solvent was removed and the crude product was purified by column chromatography (eluent: hexane/chloroform = 7/3) followed by recrystallization from hexane/ethanol to afford orange solid (0.45 g, 1.5 mmol, yield = 75%). ^{1}H NMR (400 MHz; $CDCl_3$; TMS): δ 7.13−7.16 (m, 4H, 5,6-*H*(isothianaphthene), 4,4′-*H*(thiophene)), 7.35 (dd, 2H, 3,3′-*H*(thiophene), J = 1.6, 3.6 Hz), 7.37 (dd, 2H, 5,5′-*H*(thiophene), J = 1.6, 5.2 Hz), 7.94 (dd, 2H, 4,7-*H*(isothianaphthene), J = 3.2, 6.8 Hz). ^{13}C NMR (100 MHz; $CDCl_3$; TMS): δ 121.51, 124.78, 125.54, 125.59, 126.49, 127.88, 135.26, 135.59.

2,2′-Bis(3,4-ethylnenedioxythiophene) (bis-EDOT). To a solution of 3,4-ethylenedioxythiophene (2.84 g, 20 mmol) in dried THF (70 mL) was added *n*-butyllithium (1.6 M in hexane) (12.5 mL, 20 mmol) dropwise over 5 min at −78 °C. After stirring at −78 °C for 1 h, $CuCl_2$ (2.69 g, 20 mmol) was added in one portion, and the mixture was gradually warmed up to room temperature over 2 h. Water (30 mL) and triethylamine (10 mL) was added. The mixture was extracted with chloroform and the organic layer was dried over magnesium sulfate. The crude compound was passed through a short plug of silica (neutralized with triethylamine) by using chloroform as an eluent. The chloroform solution (300 mL) was poured into hot hexane (700 mL) and cooled in 0 °C. The precipitate was collected by filtration to afford a light green yellow solid (1.53 g, 5.43 mmol, yield = 54%). ^{1}H NMR (400 MHz; $CDCl_3$; TMS): δ 4.23−4.34 (m, 8H, −O−C_2H_4−O−), 6.27 (s, 2H, *H*(thiophene). ^{13}C NMR (100 MHz; $CDCl_3$; TMS): δ 141.20, 136.99, 109.88, 97.51, 64.99, 64.59.

3-Bromothiophene-2-carbaldehyde (7). 3-Bromothiophene (20.0 g, 122.7 mmol) was added dropwise to a solution of lithium diisopropylamide (freshly prepared from diisopropylamine (17.2 mL, 122.7 mmol) and 1.6 M *n*-butyllithium (76.7 mL, 122.7 mmol) in tetrahydrofuran (210 mL)) at 0 °C. After stirring the mixture for 1 h, dimethylformamide (9.5 mL, 122.7 mmol) was added to the mixture at 0 °C and the mixture was warmed up to room temperature. After stirring fo r 4 h, water (100 mL) was added to the mixture and extracted with ether three times. The organic layer was dried over magnesium sulfate. Evaporating in vacuo to afford a pale tan liquid (21.7 g, 113.8 mmol, yield = 93%). ^{1}H NMR (400 MHz; $CDCl_3$; TMS): δ 7.16 (d, 1H, J = 4.8 Hz), 7.72 (dd, 1H, J = 1.2, 5.2 Hz), 9.99 (d, 1H, J = 1.2 Hz). ^{13}C NMR (100 MHz; $CDCl_3$; TMS): δ 120.37, 132.04, 134.84, 136.91, 183.01.

Ethyl Thieno[3,2-*b*]thiophene-2-carboxylate (8). 3-Bromothiophene-2-carbaldehyde (**7**) (21.0 g, 110 mmol) was added to a mixture of potassium carbonate (20.7 g, 150 mmol) and 2-sulfanyl acetate (13.8 g, 115 mmol) in dimethylformamide (200 mL) at room temperature. After stirring for 3 days at room temperature, the mixture was poured into water (600 mL) and extracted with dichloromethane. The organic layer was dried over magnesium sulfate. The crude product was purified by silica gel column chromatography (eluent: dichloromethane) to afford a yellow liquid (21.3 g, 100 mmol, yield = 91%). ^{1}H NMR (400 MHz; $CDCl_3$; TMS): δ 1.40 (t, 3H, J = 7.0 Hz), 4.39 (quartet, 2H, J = 7.0 Hz), 7.28 (d, 1H, J = 5.8 Hz), 7.58 (d, 1H, J = 5.8 Hz), 7.99 (s, 1H). ^{13}C NMR (100 MHz; $CDCl_3$; TMS): δ 14.36, 61.38, 119.75, 125.57, 131.61,135.19, 138.72, 143.88, 162.69.

Thieno[3,2-*b*]thiophene-2-carboxylic Acid (9). A solution of ethyl thieno[3,2-*b*]thiophene-2-carboxylate (**8**) (21.39 g, 100 mmol) and lithium hydroxide monohydrate (8.39 g, 200 mmol) in tetrahydrofuran (200 mL) and water (200 mL) was refluxed at 100 °C for 4 h. After the reaction, the solvent was evaporated, and concentrated HCl was added to the residue. The precipitate was extracted with chloroform and water. The organic layer was dried over magnesium sulfate. Removing the solvent under reduced pressure gave a white solid (18.03 g, 97.8 mmol, yield = 98%). ^{1}H NMR (400 MHz; $CDCl_3$; TMS): δ 7.32 (d, 1H, J = 5.0 Hz), 7.65 (d, 1H, J = 5.0 Hz), 8.10 (s, 1H). ^{13}C NMR (100 MHz; $CDCl_3$; TMS): δ 119.83, 127.33, 132.66, 133.67, 138.93, 145.19, 167.35.

Thieno[3,2-*b*]thiophene (TT). A solution of thieno[3,2-*b*]-thiophene-2-carboxylic acid (**9**) (9.21 g, 50.0 mmol) and copper (2.00 g,) in quinoline (80 mL) was refluxed at 260 °C to generate carbon dioxide gas. After 30 min of reaction, the solution was cooled to room temperature and extracted with ether and washed thoroughly with 1 M HCl(aq). The organic layer was dried over magnesium sulfate. The crude product was purified by silica gel column chromatography (eluent: hexane) to afford a white solid (5.75 g, 41.0 mmol, yield = 82%). ^{1}H NMR (400 MHz; $CDCl_3$; TMS): δ 7.26 (d, 1H, J = 5.0 Hz), 7.38 (d, 1H, J = 5.0 Hz). ^{13}C NMR (100 MHz; $CDCl_3$; TMS): δ 119.34, 127.32, 139.41.

5-Tributylstannylthieno[3,2-*b*]thiophene (10). To a solution of thieno[3,2-*b*]thiophene (**TT**) (1.40 g, 10.0 mmol) in tetrahydrofuran (50 mL) was added 1.6 M *n*-butyllithium (6.25 mL, 10.0 mmol) dropwise at −78 °C. After stirring at −78 °C for 1 h, tributylstannyl chloride (3.58 g, 11.0 mmol) was added to the mixture at −78 °C, and the mixture was gradually warmed up to room temperature. After stirring for 4 h, the reaction was quenched with water (50 mL). The mixture was extracted with ether, and the organic layer was dried over magnesium sulfate. Removing the solvent under reduced pressure gave a tan oil (4.08 g, 9.5 mmol, yield = 95%). ^{1}H NMR (400 MHz; $CDCl_3$; TMS): δ 0.90 (t, 9H, J = 7.2 Hz), 1.12−1.16 (m, 6H), 1.31−1.40 (m, 6H), 1.55−1.63 (m, 6H), 7.23 (d, 1H, J = 5.6 Hz), 7.26 (s, 1H), 7.34 (d, 1H, J = 5.6 Hz). ^{13}C NMR (100 MHz; $CDCl_3$; TMS): δ 10.91, 13.67, 27.28, 28.95, 118.99, 126.53, 126.98, 140.64, 141.57, 145.26.

4,7-Dibromobenzo[1,2,5]thiadiazole (11). To a solution of benzo[1,2,5]thiadiazole (6.81 g, 50 mmol) in 47% hydrobromic acid(aq) (100 mL) was added a solution of bromine (25 g, 156.4 mmol) in 47% hydrobromic acid (aqueous) (75 mL) through a dropping funnel over 1 h at room temperature, then the mixture was refluxed at 100 °C. After 6 h, the mixture was cooled to room temperature, and sodium thiosulfate aqueous solution was added to the mixture. The precipitate was recover by filtration, and purified by silica gel column chromatography (eluent: dichloromethane) to afford a pale yellow solid (12.90 g, 43.9 mmol, yield = 88%). ^{1}H NMR (400 MHz; $CDCl_3$; TMS): δ 7.73 (s, 1H). ^{13}C NMR (100 MHz; $CDCl_3$; TMS): δ 113.90, 132.35, 152.94.

4,7-Di(2-furyl)benzo[1,2,5]thiadiazole (F-Btdaz). A solution of 2-tributylstannylfuran (0.75 g, 2.1 mmol), 4,7-dibromo-benzo[1,2,5]-thiadiazole (**11**) (0.29 g, 1.0 mmol), and $Pd(PPh_3)_4$ (0.023 g, 0.020 mmol) in toluene (4 mL) was refluxed at 90 °C for 24 h. After cooling to room temperature, the mixture was purified silica gel column chromatography (contain 10% v/v of potassium carbonate) (eluent: chloroform/hexane = 1/1) and recrystallized from hexane to afford a red solid (0.18 g, 0.68 mmol, yield = 68%). ^{1}H NMR (400 MHz; $CDCl_3$; TMS): δ 6.63 (dd, 2H, J = 3.6, 4.8 Hz), 7.58 (dd, 2H, J = 0.8, 4.8 Hz), 7.67 (dd, 2H, J = 0.8, 3.6 Hz), 8.04 (s, 2H). ^{13}C NMR (100 MHz; $CDCl_3$; TMS): δ 112.14, 112.47, 121.76, 123.50, 142.79, 150.13, 151.30.

4,7-Di(2-thienyl)-benzo[1,2,5]thiadiazole (T-Btdaz). A solution of 2-tributylstannylthiophene (0.78 g, 2.1 mmol), 4,7-dibromo-benzo[1,2,5]thiadiazole (**11**) (0.29 g, 1.0 mmol), and $Pd(PPh_3)_4$ (0.023 g, 0.020 mmol) in toluene (4 mL) was refluxed at 90 °C for 24 h. After cooling to room temperature, the mixture was purified silica gel column chromatography (contain 10% v/v of potassium carbonate) (eluent: chloroform/hexane = 1/2) and recrystallized from hexane to afford an orange solid (0.19 g, 0.62 mmol, yield = 62%). ^{1}H NMR (400 MHz; $CDCl_3$; TMS): δ 7.22 (dd, 2H, J = 3.7, 5.1 Hz), 7.46 (dd, 2H, J = 1.2, 5.1 Hz), 7.87 (s, 2H), 8.12 (dd, 2H, J = 1.2, 3.7 Hz).

dx.doi.org/10.1021/ma400302j | *Macromolecules* XXXX, XXX, XXX−XXX

^{13}C NMR (100 MHz; $CDCl_3$; TMS): δ 125.79, 125.99, 126.81, 127.50, 128.01, 139.34, 152. 63.

4,7-Bis[thieno[3,2-*b*]thiophen-2-yl]benzo[1,2,5]thiadiazole (TT-Btdaz). A solution of 2-tributylstannyl-thieno[3,2-*b*]thiophene (**10**) (0.90 g, 2.1 mmol), 4,7-dibromo-benzo[1,2,5]thiadiazole (**11**) (0.29 g, 1.0 mmol), and $Pd(PPh_3)_4$ (0.023 g, 0.020 mmol) in toluene (10 mL) was refluxed at 90 °C for 24 h. After cooling to room temperature, the mixture was purified silica gel column chromatography (contain 10% v/v of potassium carbonate) (eluent: tetrahydrofuran) and recrystallized from chloroform/hexane to afford a purple solid (0.20 g, 0.49 mmol, yield = 49%). ^{1}H NMR (400 MHz; $CDCl_3$; TMS): δ 7.31 (d, 2H, J = 5.0 Hz), 7.46 (d, 2H, J = 5.0 Hz), 7.88 (s, 2H), 8.50 (s, 1H). ^{13}C NMR (100 MHz; $CDCl_3$; TMS): δ 119.57, 120.62, 125.66, 126.51, 128.44, 139.65, 140.43, 141.21, 152.58.

2,7-Di(2-thienyl)fluorene (T-Fl). A solution of 2-tributylstannylthiophene (1.40 g, 3.7 mmol), 2,7-dibromofluorene (0.59 g, 1.8 mmol), and $Pd(PPh_3)_4$ (0.040 g, 0.035 mmol) in toluene (4 mL) was refluxed at 90 °C for 24 h. After cooling to room temperature, the mixture was purified silica gel column chromatography (contain 10% v/v of potassium carbonate) (eluent: dichloromethane) and recrystallized from chloroform to afford a pale brown solid (0.35 g, 1.05 mmol, yield = 58%). ^{1}H NMR (400 MHz; $CDCl_3$; TMS): δ 3.98 (s, 2H), 7.10 (dd, 2H, J = 3.6, 5.1 Hz), 7.29 (dd, 2H, J = 1.2, 5.1 Hz), 7.37 (dd, 2H, J = 1.2, 3.6 Hz), 7.65 (dd, 2H, J = 1.3, 8.0 Hz), 7.77 (d, 2H, J = 8.0 Hz), 7.80 (d, 2H, J = 1.3 Hz). ^{13}C NMR (100 MHz; $CDCl_3$; TMS): δ 36.92, 120.25, 122.54, 122.93, 124.62, 124.96, 128.09, 133.07, 140.74, 144.16, 144.86.

4,4′-Di(2-thienyl)biphenyl (T-Bp). A solution of 2-tributylstannylthiophene (0.78 g, 2.1 mmol), 4,4′-diromobiphenyl (0.31 g, 1.0 mmol), and $Pd(PPh_3)_4$ (0.023 g, 0.020 mmol) in toluene (8 mL) were refluxed at 90 °C for 24 h. After cooling to room temperature, the mixture was purified silica gel column chromatography (contain 10% v/v of potassium carbonate) (eluent: chloroform) and recrystallized from chloroform to afford a white solid (0.22 g, 0.69 mmol, yield = 69%). ^{1}H NMR (400 MHz; $CDCl_3$; TMS): δ 7.11 (dd, 2H, J = 3.4, 5.2 Hz), 7.31 (dd, 2H, J = 1.0, 5.2 Hz), 7.37 (dd, 2H, J = 1.0, 3.4 Hz), 7.64 (d, 2H, J = 8.6 Hz), 7.71 (d, 2H, J = 8.6 Hz). ^{13}C NMR (100 MHz; $CDCl_3$; TMS): δ 123.19, 125.08, 126.44, 127.21, 128.01, 133.57, 139.46, 144.10.

3,6-Dibromo-*N*-methylcarbazole (12). A solution of 3,6-dibromocarbazole (0.39 g, 1.2 mmol), iodomethane (0.28 g, 2.0 mmol), and potassium carbonate (0.28 g, 2.0 mmol) in acetone (3 mL) was stirred at room temperature. After 24 h, the mixture was extracted with dichloromethane and water, and the organic layer was dried over magnesium sulfate. The crude product was purified by silica gel column chromatography (eluent: chloroform/hexane = 1/4) to afford a white solid (0.24 g, 0.69 mmol, yield = 58%). ^{1}H NMR (400 MHz; $CDCl_3$; TMS): δ 3.80 (s, 3H,), 7.25 (d, 2H, J = 8.6 Hz), 7.56 (dd, 2H, J = 1.8, 8.6 Hz), 8.12 (d, 2H, J = 1.8 Hz). ^{13}C NMR (100 MHz; $CDCl_3$; TMS): δ 29.32, 110.13, 112.05, 123.18, 123.33, 129.06, 139.82.

***N*-Methyl-3,6-di(2-thienyl)carbazole (3,6T-Cz1).** A solution of 2-tributylstannylthiophene (0.51 g, 1.36 mmol), 3,6-dibromo-*N*-methylcarbazole (**12**) (0.22 g, 0.65 mmol), and $Pd(PPh_3)_4$ (0.016 g, 0.014 mmol) in toluene (3 mL) was refluxed at 90 °C for 24 h. After cooling to room temperature, the mixture was purified silica gel column chromatography (contain 10% v/v of potassium carbonate) (eluent: chloroform/hexane = 3/7) to afford a white solid (0.13 g, 0.36 mmol, yield = 56%). ^{1}H NMR (400 MHz; $CDCl_3$; TMS): δ 7.11 (dd, 2H, J = 3.6, 5.2 Hz), 7.27 (dd, 2H, J = 1.2, 5.2 Hz), 7.35−7.38 (m, 4H), 7.75 (dd, 2H, J = 2.0, 4.8 Hz), 8.33 (d, 2H, J = 1.6 Hz). ^{13}C NMR (100 MHz; $CDCl_3$; TMS): δ 29.31, 108.92, 117.93, 122.12, 123.13, 123.73, 124.64, 126.00, 128.00, 140.95, 145.60.

Dibenzothiophene 5,5-Dioxide (13). A solution of dibenzothiophene (9.21 g, 50.0 mmol) and 33% H_2O_2(aq) (25 mL) in acetic acid (150 mL) was refluxed at 130 °C. After 4 h, the mixture was cooled to room temperature and cooled in a fridge. The precipitate was filtered to give a white solid (10.15 g, 46.9 mmol, yield = 94%). ^{1}H NMR (400 MHz; $CDCl_3$; TMS): δ 7.53 (dt, 2H, J = 1.2, 7.6 Hz), 7.64 (dt, 2H, J = 1.2, 7.6 Hz), 7.79 (d, 2H, J = 7.6 Hz), 7.83 (d, 2H, J = 7.6 Hz). ^{13}C NMR (100 MHz; $CDCl_3$; TMS): δ 121.60, 122.17, 130.39, 131.60, 133.90, 137.66.

3,7-Dibromodibenzothiophene 5,5-Dioxide (14). To a solution of dibenzothiophene 5,5-dioxide (**13**) (9.73 g, 45 mmol) in concentrated H_2SO_4 (330 mL) was added dibromoisocyanuric acid (14.9 g, 52 mmol) in one portion at room temperature. After stirring for 20 h, the mixture was poured into ice water (1000 mL). The white precipitate was filtered. The filter cake was washed with 5% NaOH(aq)/chloroform, and the organic layer was dried over magnesium sulfate. The crude product was recrystallized from chloroform to afford white solid (6.95 g, 18.6 mmol, yield = 41%). ^{1}H NMR (400 MHz; $CDCl_3$; TMS): δ 7.64 (d, 2H, J = 8.1 Hz), 7.77 (dd, 2H, J = 1.7, 8.1 Hz), 7.94 (d, 2H, J = 1.7 Hz). ^{13}C NMR (100 MHz; $CDCl_3$; TMS): δ 122.92, 124.60, 125.58, 129.58, 137.15, 138.87.

3,7-Dibromodibenzothiophene (15). To a solution of 3,7-Dibromo-dibenzothiophene 5,5-dioxide (**14**) (4.00 g, 10.7 mmol) in ether (100 mL) was added lithium aluminum hydride (2.00 g, 52.7 mmol) slowly over 10 min at room temperature. After gently refluxing for 4 h, the mixture was cooled to room temperature, and 3 mL of water and concentrated HCl (10 mL) was carefully added to the mixture in turn. The precipitate was filtered off and washed thoroughly with dichloromethane. The crude product was purified by silica gel column chromatography (eluent: ethyl acetate) followed by recrystallization from chloroform/ethanol to afford a white solid (1.90 g, 5.6 mmol, yield = 52%). ^{1}H NMR (400 MHz; $CDCl_3$; TMS): δ 7.56 (d, 2H, J = 7.6 Hz), 7.93−7.96 (m, 4H). ^{13}C NMR (100 MHz; $CDCl_3$; TMS): δ 120.82, 122.62, 125.49, 128.18, 133.75, 140.94.

3,7-Di(2-furyl)dibenzothiophene (F-Dbt). A solution of 2-tributylstannylfuran (0.75 g, 2.1 mmol), 3,7-dibromodibenzothiophene (0.34 g, 1.0 mmol), and $Pd(PPh_3)_4$ (0.023 g, 0.020 mmol) in toluene (8 mL) was refluxed at 90 °C for 24 h. After cooling to room temperature, the mixture was purified silica gel column chromatography (contain 10% v/v of potassium carbonate) (eluent: chloroform) and recrystallized from chloroform/hexane to afford a pale yellow solid (0.17 g, 0.54 mmol, yield = 54%). ^{1}H NMR (400 MHz; $CDCl_3$; TMS): δ 6.53 (dd, 2H, J = 1.6, 3.2 Hz), 6.76 (d, 2H, J = 3.2 Hz), 7.52 (d, 2H, J = 1.6 Hz), 7.76 (dd, 2H, J = 1.5, 8.2 Hz), 8.11 (d, 2H, J = 8.8 Hz), 8.15 (d, 2H, J = 1.5 Hz). ^{13}C NMR (100 MHz; $CDCl_3$; TMS): δ 105.66, 111.91, 117.70, 120.73, 121.69, 129.46, 134.33, 140.36, 142.39, 153.67.

3,7-Di(2-thienyl)dibenzothiophene (T-Dbt). A solution of 2-tributylstannylthiophene (0.78 g, 2.1 mmol), 3,7-dibromodibenzothiophene (0.34 g, 1.0 mmol), and $Pd(PPh_3)_4$ (0.023 g, 0.020 mmol) in toluene (10 mL) was refluxed at 90 °C for 24 h. After cooling to room temperature, the mixture was purified silica gel column chromatography (contain 10% v/v of potassium carbonate) (eluent: chloroform) and recrystallized from chloroform/hexane to afford a white solid (0.22 g, 0.62 mmol, yield = 62%). ^{1}H NMR (400 MHz; $CDCl_3$; TMS): δ 7.12 (dd, 2H, J = 3.8, 5.0 Hz), 7.32 (d, 2H, J = 4.8 Hz), 7.41 (d, 2H, J = 3.6 Hz), 7.71 (dd, 2H, J = 1.4, 8.2 Hz), 8.07 (d, 2H, J = 1.2 Hz), 8.10 (d, 2H, J = 8.4 Hz). ^{13}C NMR (100 MHz; $CDCl_3$; TMS): δ 114.67, 119.91, 121.87, 123.08, 123.64, 125.28, 128.21, 133.38, 140.65, 144.19.

SYNTHESIS OF CHIRAL INDUCERS

Synthetic routes of chiral inducer were described in Scheme 2.

4′-Hydroxybiphenyl-4-carboxylic Acid (16). A suspension of 4-cyano-4′-hydroxybiphenyl (9.76 g, 50 mmol) and sodium hydroxide (10.00 g, 250 mmol) in ethanol (50 mL) and water (300 mL) were refluxed at 120 °C for 24 h. After the reaction, the mixture was cooled to room temperature and poured into 500 mL of water. Hydrochloric acid was added into the mixture with vigorous stirring until pH was around 1 to precipitate white solid. The resulting white precipitate was recovered by vacuum filtration to afford white solid (10.42 g, 48.6 mmol, yield = 97%). ^{1}H NMR (400 MHz; DMSO-d_6; TMS): δ 6.96 (d, 2H, J = 8.6 Hz), 7.66 (d, 2H, J = 8.6 Hz), 7.89

dx.doi.org/10.1021/ma400302j | *Macromolecules* XXXX, XXX, XXX−XXX

(d, 2H, J = 8.2 Hz), 8.05 (d, 2H, J = 8.2 Hz), 9.81 (s, 1H). ^{13}C NMR (100 MHz; $CDCl_3$; TMS): δ 115.87, 125.83, 128.12, 128.52, 129.60, 129.91, 144.31, 157.90, 167.23.

4′-Hydroxybiphenyl-4-carboxylic Acid (*S*)-1-Methyl-Heptyl Ester (17*S*). To a solution of 4′-hydroxy-biphenyl-4-carboxylic acid (**16**) (3.21 g, 15.0 mmol), triphenylphosphine (3.99 g, 15.2 mmol), and (*R*)-2-octanol (1.98 g, 15.2 mmol) in THF (20 mL) was added diisopropyl azodicarboxylate (40% in toluene) (3.07 g, 15.2 mmol) dropwise at 0 °C. After stirring for 12 h, the solvent was evaporated. The crude product was purified by silica gel column chromatography (eluent: chloroform/ethyl acetate = 9/1) to afford white solid (4.19 g, 12.8 mmol, yield = 85.6%). ^{1}H NMR (400 MHz; $CDCl_3$; TMS): δ 0.86 (t, 3H, J = 6.6 Hz), 1.27- 1.43 (m, 11H), 1.58−1.79 (m, 2H), 5.18 (sextet, 1H, J = 5.8 Hz), 5.49 (s, 1H), 6.95 (d, 2H, J = 8.4 Hz), 7.52 (d, 2H, J = 8.4 Hz), 7.60 (d, 2H, J = 8.4 Hz), 8.08 (d, 2H, J = 8.4 Hz). ^{13}C NMR (100 MHz; $CDCl_3$; TMS): δ 14.05, 20.10, 22.58, 25.41, 29.16, 31.73, 36.07, 71.89, 115.84, 126.41, 128.57, 128.91, 130.04, 132.59, 145.08, 155.99, 166.44.

4′-(4-Hexyloxybenzoyloxy)biphenyl-4-carboxylic Acid (*S*)-1-Methylheptyl Ester ((*S*)-8BpB6). To a solution of 4-hexyloxybenzoic acid (0.91 g, 5.0 mmol) and *N*,*N*′-dicyclohexylcarbodiimide (1.03 g, 5.0 mmol) in dichloromathane (15 mL) was added a solution of 4′-hydroxy-biphenyl-4-carboxylic acid-(*S*)-1-methyl-heptyl ester (**17*S***) (1.31 g, 4.0 mmol) and *N*,*N*-dimethyl-4-aminopyridin (0.61 g, 5.0 mmol) in dichloromathane (15 mL) dropwise over 1 h. After stirring for 20 h at room temperature, white precipitate was removed by filtration. The crude product was purified by silica gel column chromatography (eluent: chloroform) followed by recrystallization from hexane/ethanol to afford white solid (1.81 g, 3.4 mmol, yield = 85.2%). ^{1}H NMR (400 MHz; $CDCl_3$; TMS): δ 0.86−0.94 (m, 6H), 1.29−1.86 (m, 21H), 4.05 (t, 2H, J = 6.6 Hz), 5.18 (sextet, 1H, J = 6.3 Hz), 6.98 (d, 2H, J = 8.8 Hz), 7.31 (d, 2H, J = 8.8 Hz), 7.65 (d, 2H, J = 8.6 Hz), 7.66 (d, 2H, J = 8.8 Hz), 8.11 (d, 2H, J = 8.6 Hz), 8.16 (m, 2H, J = 8.8 Hz). ^{13}C NMR (100 MHz; $CDCl_3$; TMS): δ 14.03, 14.08, 20.12, 22.60, 25.47, 25.67, 29.08, 29.19, 31.56, 31.77, 34.94, 36.11, 68.36, 71.81, 114.35, 121.38, 122.32, 126.95, 128.35, 129.76, 130.09, 132.34, 137.70, 144.65, 151.18, 163.66, 164.92, 166.07.

■ ASSOCIATED CONTENT

Ⓢ Supporting Information

General methods, calculated spin density of the monomers in radical cationic state, DSC curves for the CLC electrolyte solutions, IR and MALDI−TOF−MS spectra of the polymers, optimized geometry of the model oligomers, POM images for the contact method, and an LD spectrum of **poly(BT)**. This material is available free of charge via the Internet at http://pubs.acs.org.

■ AUTHOR INFORMATION

Corresponding Author

*E-mail: gotoh@ims.tsukuba.ac.jp. Telephone: +81-29-853-5128. Fax: +81-29-853-4490.

Notes

The authors declare no competing financial interest.

■ ACKNOWLEDGMENTS

We would like to thank Chemical Analysis Center of University of Tsukuba and Glass Work Shop of University of Tsukuba. This research was supported by the Japan Society for the Promotion of Science, Grant in-Aid for Scientific Research, 22550161. K.K. is a research fellow of the Japan Society for the Promotion of Science.

■ ABBREVIATIONS

CLC, cholesteric liquid crystal; CD, circular dichroism; BT, 2,2′-bithiophene; ter-T, 2,2′:5′,2″-terthiophene; 3DMBT, 3,3′-dimethyl-2,2′-bithiophene; 4DMBT, 4,4′-dimethil-2,2′-bithiophene; TMBT, 3,4,3′,4′-tetramethyl-2,2′-bithiphene; T-ITN, 1,3-di(2-thienyl)isothianaphthene; EDOT, 3,4-ethylenedioxythiophene; bis-EDOT, 2,2′-bis(3,4-ethylnenedioxythiophene); TT, thieno[3,2-*b*]thiophene; bis-TT, 2,2′-bithieno[3,2-*b*]-thiophene; T-Fl, 2,7-di(2-thienyl)fluorene; T-Cz1, *N*-methyl-2,7-di(2-thienyl)carbazole; T-Dbt, 3,7-di(2-thienyl)-dibenzothiophene; T-Bp, 4,4′-di(2-thienyl)biphenyl; F-Fl, 2,7-di(2-furyl)fluorene; F-Cz1, *N*-methyl-2,7-di(2-furyl)carbazole; F-Dbt, 3,7-di(2-furyl)dibenzothiophene; F-Bp, 4,4′-di(2-furyl)-biphenyl; T-Btdaz, 4,7-di(2-thienyl)-benzo[1,2,5]thiadiazole; F-Btdaz, 4,7-di(2-furyl)-benzo[1,2,5]thiadiazole; TT-Btdaz, 4,7-bis-thieno[3,2-*b*]thiophen-2-yl-benzo[1,2,5]thiadiazole; 3,6T-Cz1, *N*-methyl-3,6-di(2-thienyl)carbazole; DFT, density functional theory; NLC, nematic liquid crystal; COC, cholesteryl oleyl carbonate; 6CB, 4-cyano-4′-*n*-hexyl biphenyl; TBAP, tetrabutylammonium perchlorate; POM, polarizing optical microscopy; DSC, differential scanning calorimetry; ITO, indium−tin−oxide; MALDI-TOF-MS, matrix-assisted laser desorption ionization time-of-flight mass spectroscopy; L/D, length/diameter; CP, cholesteryl pelargonate

■ REFERENCES

(1) Wulff, G. *Angew. Chem., Int. Ed.* **1989**, *28*, 21−37.
(2) Nakano, T. *J. Chromatogr. A* **2001**, *906*, 205−225.
(3) Kauranen, M.; Verbiest, T.; Boutton, C.; Teerenstra, M. N.; Clays, K.; Schouten, A. J.; Nolte, R. J. M.; Persoons, A. *Science* **1995**, *270*, 966−969.
(4) Hu, Q.; Huang, W.; Vitharana, D.; Zheng, X.; Pu, L. *J. Am. Chem. Soc.* **1997**, *119*, 12454−12464.
(5) Song, F.; Wei, G.; Wang, L.; Jiao, J.; Cheng, Y.; Zhu, C. *J. Org. Chem.* **2012**, *77*, 4759−4764.
(6) Pu, L. *Acta Polym.* **1997**, *48*, 116−141.
(7) Beaujjge, P. M.; Ellinger, S.; Reynolds, J. R. *Nature Mat.* **2008**, *7*, 795−799.
(8) Roncali, J. *Chem. Rev.* **1997**, *97*, 173−205.
(9) Grem, G.; Leditzky, G.; Ullrich, B.; Leising, G. *Adv. Mater.* **1992**, *4*, 36−37.
(10) Grice, A. W.; Bradley, D. D. C.; Bernius, M. T.; Inbasekaran, M.; Wu, W. W.; Woo, E. P. *Appl. Phys. Lett.* **1998**, *73*, 629−631.
(11) Morin, J. F.; Beaupré, S.; Leclerc, M.; Lévesque, I.; D'lorio, M. *Appl. Phys. Lett.* **2002**, *80*, 341−343.
(12) Xu, B.; Holdcroft, S. *Macromolecules* **1993**, *26*, 4457−4460.
(13) Groenendaal, L. B.; Jonas, F.; Freitag, D.; Pielartzik, H.; Reynolds, J. R. *Adv. Mater.* **2000**, *12*, 481−494.
(14) Hagan, A. J.; Moratti, S. C.; Sage, I. C. *Synth. Met.* **2001**, *119*, 147−148.
(15) Nomura, R.; Tabei, J.; Nishiura, S.; Masuda, T. *Macromolecules* **2003**, *36*, 561−564.
(16) Schwartz, E.; Koepf, M.; Kitto, H. J.; Nolte, R. J. M.; Rowan, A. E. *Polym. Chem.* **2011**, *2*, 33−47.
(17) Langeveld-Voss, B. M. W.; Janssen, R. A. J.; Christiaans, M. P. T.; Meskers, S. C. J.; Dekkers, H. P. J. M.; Meijer, E. W. *J. Am. Chem. Soc.* **1996**, *118*, 4908−4909.
(18) Nilsson, K. P. R.; Olsson, J. D. M.; Konradsson, P.; Inganäs, O. *Macromolecules* **2004**, *37*, 6316−6321.
(19) Yashima, E.; Goto, H.; Okamoto, Y. *Macromolecules* **1999**, *32*, 7942−7945.

(20) Yan, J.; Cheng, X.; Zhou, Q.; Pei, J. *Macromolecules* **2007**, *40*, 832−839.
(21) Goto, H. *Phys. Rev. Lett.* **2007**, *98*, 253901.
(22) Genies, E. M.; Bidan, G.; Diaz, A. F. *J. Electroanal. Chem.* **1983**, *149*, 101−113.
(23) Waltman, R. J.; Bargon, J. *Can. J. Chem.* **1985**, *64*, 76−95.
(24) Yoneyama, H.; Tsujimoto, A.; Goto, H. *Macromolecules* **2007**, *40*, 5279−5283.
(25) Wang, Y.; Li, Q. *Adv. Mater.* **2012**, *24*, 1926−1945.
(26) Goto, H. *Adv. Funct. Mater.* **2009**, *19*, 1−8.
(27) Roncali, J. *Chem. Rev.* **1992**, *92*, 711−738.
(28) Bidan, G.; Guillerez, S.; Sorokin, V. *Adv. Mater.* **1996**, *8*, 157−160.
(29) Langeveld-Voss, B. M. W.; Christiaans, M. P. T.; Janssen, R. A. J.; Meijer, E. W. *Macromolecules* **1998**, *31*, 6702−6704.
(30) Berova, N.; Nakanishi, K.; Woody, R. W. *Circular Dichroism: Principles and Applications*, 2nd ed.; Wiley: New York, 2000.
(31) Krische, B.; Hellberg, J.; Lilja, C. *J. Chem. Soc., Chem. Commun.* **1987**, *19*, 1476−1478.
(32) Kawabata, K.; Goto, H. *Synth. Met.* **2010**, *160*, 2290−2298.
(33) Kawabata, K.; Goto, H. *Chem.—Eur. J.* **2012**, *18*, 15065−15072.
(34) Yoneyama, H.; Kawabata, K.; Tsujimoto, A.; Goto, H. *Electrochem. Commun.* **2008**, *10*, 965−969.
(35) Goto, H.; Kawabata, K. *Polym. Chem.* **2011**, *2*, 1098−1106.